Combination of Polarized TIRF and ATR Spectroscopies for Determination of the Second and Fourth Order Parameters of Molecular Orientation in Thin Films and Construction of an Orientation Distribution Based on the Maximum Entropy Method

Anne F. Runge,[†] S. Scott Saavedra,[†] and Sergio B. Mendes*,[†,‡]

Department of Chemistry and College of Optical Sciences, University of Arizona, Tucson, Arizona 85721

Received: October 21, 2005; In Final Form: January 13, 2006

This article describes two mathematical formalisms for the determination of the second and fourth order parameters of molecular films using optical spectroscopy. Method A uses polarized total internal reflection fluorescence (TIRF) to calculate the second and fourth order parameters, $\langle P_2(\cos \theta)\rangle$ and $\langle P_4(\cos \theta)\rangle$, using an independently determined value for the angle between the absorption and emission dipoles, γ. Method B uses $\langle P_2(\cos \theta)\rangle$ obtained from attenuated total reflectance (ATR) data, along with polarized TIRF measurements to calculate $\langle P_4(\cos \theta)\rangle$ and $\langle\cos^2 \gamma\rangle$. The choice of a specific method should rely on experimental considerations. We also present a method to separate the contributions of substrate surface roughness and dipole orientation with respect to the molecular axis from the spectroscopically determined second and fourth order parameters. Finally, a maximum entropy approach for construction of an orientation distribution from order parameters is compared with the commonly used delta and Gaussian distributions.

1. Introduction

Molecular structure and orientation in organic thin films have a profound impact on their biological, chemical, and physical properties. Focusing on the determination of molecular orientation in thin films, it is important to divide the goal into two major tasks. The first task is to extract orientation order parameters from experimental measurements of the film. This task depends on the information content of the experimental technique being employed (for example, if it is a one-photon or two-photon process) and defines the geometric information (order parameter) that a particular optical spectroscopic technique can provide. Typically, the information obtained here is the ensemble average of a particular spherical harmonic function (or an even Legendre polynomial term, $\langle P_{2n}(\cos \theta)\rangle$, if the film is uniaxial). The second task is to use these order parameters to construct an orientation distribution. Order parameters are typically limited to a few discrete pieces of information, and a model is necessary to construct an orientation distribution that can potentially determine an infinite number of order parameters. Both tasks above have been the subject of much theoretical and experimental research over the past 30 years.

In general, the second order parameter, $\langle P_2(\cos \theta)\rangle$, can be determined by methods such as polarized IR, UV, or visible absorption spectroscopies, which are techniques involving the annihilation of one photon.[1−7] Nonlinear optical techniques such as sum frequency generation and second harmonic generation have also been used to measure the third order parameter of non-centrosymmetric assemblies, as described in the work of Shen et al.[8,9] Techniques based on two-photon processes such as Raman scattering[2,10−13] and fluorescence emission contain information that can be related to the second and fourth order
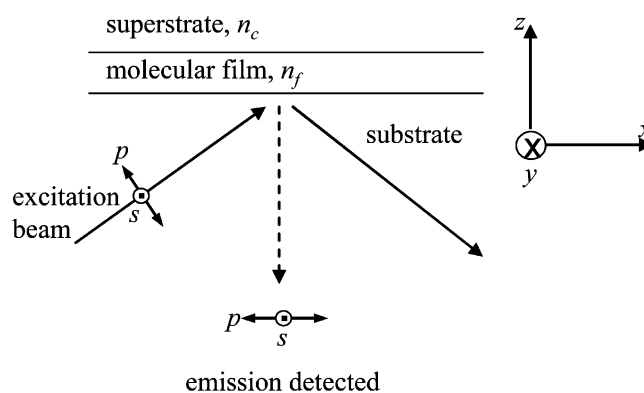

Figure 1. Configuration for polarized TIRF experiments. Fluorescence in the molecular film is excited by the optical field of an incoming light beam incident in the x−z plane, which is polarized at either s or p. Fluorescence is detected normal to the substrate, and a polarizer in the detection path selects either s or p emission relative to the plane of incidence (x−z plane). The molecular film with a refractive index of n_f is between the substrate and the superstrate, which has a refractive index of n_c.

parameters. Relevant to our work, we will focus in this introduction on the determination of order parameters from fluorescence emission.

Chapoy and DuPrè[14,15] calculated order parameters from polarized fluorescence measurements for a geometry where the optical beam could be polarized for both the excitation and emission processes along the major axis of symmetry (z-axis) of an optically uniaxial film. However, the literature cited above is insufficient for dealing with measurements in the total internal reflection fluorescence (TIRF) geometry, as illustrated in Figure 1; in this case, the optical excitation along the axis of symmetry (z-axis) using p-polarized excitation light also involves a contribution along the x-axis and both Cartesian components need to be considered for a proper calculation of order parameters. Levine and co-workers have determined the second and fourth order parameters for fluorescent probes in lipid

* To whom correspondence should be addressed. Fax: (520) 621-8407. Voice: (520) 621-6340. E-mail: sergiom@u.arizona.edu.
† Department of Chemistry.
‡ College of Optical Sciences.

bilayers using an angle-resolved fluorescence depolarization approach, which extends to both the steady state and time resolved domains.[7,16−23] LeGrange and co-workers used polarized fluorescence to determine order parameters under the simplifying assumptions that the absorption and emission dipoles are collinear and along the molecular axis,[24,25] but those assumptions are not applicable for all molecular assemblies.

Polarized fluorescence in a TIRF geometry has been employed by several groups[26−36] to recover molecular orientation in thin-film assemblies. However, several limitations are present in the literature. In some cases,[32,35] the absorption and emission transition dipole moments are assumed to be collinear. In another case,[36] the polarization of the detected fluorescence was not considered (theoretically and experimentally) and information on both the second order parameter (from attenuated total reflectance (ATR) data) and the angle between the absorption and emission dipoles, γ, was required to produce orientation information from TIRF data. In the work of Tronin et al.,[33,34] the equations for calculating the polarized fluorescence intensities have mathematical errors that are discussed in this paper. Kleijn and co-workers[26−29] employed TIRF measurements to obtain the second and fourth order parameters of porphyrin molecules with circular symmetry under the assumption of complete depolarization in the porphyrin plane of the emission dipole relative to the absorption dipole, $\langle \cos^2 \gamma \rangle = 0.5$. In later works of Kleijn dealing with linear dipoles,[30,31] $\langle \cos^2 \gamma \rangle$ was arbitrarily chosen with the purpose of placing the order parameters inside the physical boundaries; however, this approach cannot uniquely determine $\langle \cos^2 \gamma \rangle$ (as there is a range of mathematically possible values) and lacks an experimental justification. Our method B described below overcomes this difficulty by combining polarized TIRF data with the second order parameter from ATR measurements to allow for the determination, in addition to the fourth order parameter, of an experimental value of $\langle \cos^2 \gamma \rangle$ in the physical/chemical environment of interest.

Once order parameters have been determined, several models have been used in the literature to describe an orientation distribution, such as delta distribution, Gaussian function, expansion in Legendre polynomials, and maximum entropy approach. The most common (and simplest) approach reported in the literature is to measure one order parameter, such as the absorption dichroic ratio, and use a delta function distribution (sometimes also called a narrow distribution) to determine one specific tilt angle for the whole population of molecules.[37−42] The delta distribution, where all molecules have the same geometrical configuration, is the most ordered distribution among all possible solutions that satisfies the information contained in one single order parameter. If different order parameters are measured and the ensemble being studied is not fully ordered, each order parameter will give a different tilt angle under the delta distribution assumption, showing the inconsistency and limitations of this model.

An approach employing two order parameters was used by Saavedra and co-workers[35,36] to construct a Gaussian distribution in an iterative procedure between ATR and TIRF measurements. Other groups have also used the order parameters from fluorescence and sum frequency generation to construct an orientation distribution using the Gaussian distribution as a model.[33,34,43] As will be discussed below, the Gaussian distribution with a priori shape is not capable of describing a large fraction of the physical domain of all possible values for two order parameters. Although the raw data in those reports remain

valid, the final distribution based on the Gaussian assumption fails to converge for a large number of the experimental cases. Details on inherent difficulties of the Gaussian distribution are provided later in the Discussion section of this article. Besides these difficulties, the Gaussian approach is limited to describing situations where exactly two order parameters are available and fails to provide any answer for situations where only one or more than two order parameters are available.

Several works have described the orientation distribution function as an expansion of orthogonal Legendre terms, where each term is an experimentally determined order parameter. Unlike the delta and Gaussian functions, the Legendre expansion can accommodate any number of order parameters and can describe the whole domain of possible values for the order parameters. The more terms present in the expansion, the more precisely the calculated distribution approaches the true distribution. If an infinite number of order parameters could be experimentally determined, then the orientation distribution would be described exactly. Chapoy and DuPrè[14,15] have described the orientation distribution of uniaxial liquid crystals using a truncated Legendre expansion. They proposed using experimental data to calculate order parameters that successively add information about the distribution by increasing terms in the Legendre expansion. Others have also used the Legendre expansion to construct orientation distributions.[24,25] One disadvantage to using the Legendre expansion to define an orientation distribution is that it is not a positively defined function. As a result, when only a few order parameters are used (as is the case of nearly all works in this area[44,45]), the probability density can have negative values,[46,47] which are not physically meaningful. A typical approach in statistics and in information theory is to use a maximum entropy technique to determine the most random probability function that is consistent with the information available.[48,49] The maximum entropy approach has been used by several researchers to determine an orientation distribution based on measured order parameters;[10,27,28,44,50] in addition, this method can be applied for any number of order parameters and always provides a positively defined distribution.

In this paper, we describe how polarized measurements of total internal reflection fluorescence (TIRF) are related to the second and fourth order parameters and geometric information on the angle between absorption and emission dipoles, $\langle \cos^2 \gamma \rangle$, as we consider the general situation where they can be non-collinear. We also show how polarized attenuated total reflectance (ATR), from which the second order parameter is determined, can be combined with TIRF data to solve for the fourth order parameter and $\langle \cos^2 \gamma \rangle$. Having determined the second and fourth order parameters, we describe a method to factor out surface roughness effects and the dipole orientation with respect to the molecular axis in the calculation of order parameters to allow for a clear identification of molecular orientation. Finally, we apply the maximum entropy method to the calculated order parameters to construct an orientation distribution for a molecular film and compare its results with commonly used delta and Gaussian distributions.

2. Theory

2.1. Polarized Fluorescence. By employing polarized light, TIRF can be used to extract information on the orientation order parameters of a thin film. As shown in Figure 1, an optical beam polarized in either the s- or p-polarization is totally reflected at

Molecular Orientation in Thin Films

J. Phys. Chem. B, Vol. 110, No. 13, 2006 **6723**

the substrate/film/superstrate interface and is used for excitation of fluorescent species in the molecular film. A set of detection optics collects the fluorescence signal that is emitted normal to the sample surface. In the detection path, the optical beam passes through a linear polarizer that filters the polarization of the fluorescence either perpendicular or parallel to the plane of incidence (the $x-z$ plane), s- or p-polarization, respectively. The combination of excitation and emission polarizations leads to four different measurements of fluorescent intensities, $I_{s,s}$, $I_{s,p}$, $I_{p,p}$, and $I_{p,s}$, where the first subscript refers to the excitation polarization and the second subscript refers to the emission polarization. The intensities of the fluorescence signal are given by[20,51]

$$I_{a,e} = \langle (\vec{\mu} \cdot \vec{E}_a)^2 (\vec{\nu} \cdot \hat{e}_e)^2 \rangle \quad (1)$$

where $\vec{E}_a$ is the electric field of the excitation beam, $\hat{e}_e$ is a unit vector in the direction of the detection polarizer, $\vec{\mu}$ is the optical absorption dipole, and $\vec{\nu}$ is the fluorescence emission dipole.

To relate the TIRF signals to the optical transition dipoles, we first consider a coordinate system $(x'-y'-z')$ where the absorption dipole has the following components:

$$\begin{pmatrix} \mu_{x'} \\ \mu_{y'} \\ \mu_{z'} \end{pmatrix} = \begin{pmatrix} 0 \\ 0 \\ \mu \end{pmatrix} \quad (2)$$

In this coordinate system, the emission dipole, which in the general case can be non-collinear with the absorption dipole, is described by the following components:

$$\begin{pmatrix} \nu_{x'} \\ \nu_{y'} \\ \nu_{z'} \end{pmatrix} = R(\gamma) \begin{pmatrix} 0 \\ 0 \\ \nu \end{pmatrix} \quad (3)$$

with a rotation matrix, $R(\gamma)$, defining the orientation of the emission dipole with respect to the absorption dipole:

$$R(\gamma) \equiv \begin{pmatrix} \cos\gamma & 0 & \sin\gamma \\ 0 & 1 & 0 \\ -\sin\gamma & 0 & \cos\gamma \end{pmatrix} \quad (4)$$

where γ is the angle between the absorption and emission dipoles (see Figure 2). The absorption and emission dipole vectors can be fully described in the lab coordinate system $(x-y-z)$ through a set of Euler rotation matrices, $R(\phi,\theta,\alpha)$:

$$R(\phi,\theta,\alpha) \equiv \begin{pmatrix} \cos\phi & -\sin\phi & 0 \\ \sin\phi & \cos\phi & 0 \\ 0 & 0 & 1 \end{pmatrix} \begin{pmatrix} \cos\theta & 0 & \sin\theta \\ 0 & 1 & 0 \\ -\sin\theta & 0 & \cos\theta \end{pmatrix}$$
$$\begin{pmatrix} \cos\alpha & -\sin\alpha & 0 \\ \sin\alpha & \cos\alpha & 0 \\ 0 & 0 & 1 \end{pmatrix} \quad (5)$$

$$\begin{pmatrix} \mu_x \\ \mu_y \\ \mu_z \end{pmatrix} = R(\phi,\theta,\alpha) \begin{pmatrix} \mu_{x'} \\ \mu_{y'} \\ \mu_{z'} \end{pmatrix} \quad (6)$$

$$\begin{pmatrix} \nu_x \\ \nu_y \\ \nu_z \end{pmatrix} = R(\phi,\theta,\alpha) \begin{pmatrix} \nu_{x'} \\ \nu_{y'} \\ \nu_{z'} \end{pmatrix} \quad (7)$$

where α, θ, and ϕ are defined as shown in Figure 2. By inserting the vector components into eq 1 and assuming in-plane symmetry (random in α and ϕ), we obtain

$$I_{s,s} = \langle \mu_y^2 \nu_y^2 \rangle E_y^2 = \frac{1}{16}\{[1 + 5\langle \cos^2\gamma \rangle] +$$
$$[2 - 14\langle \cos^2\gamma \rangle]\langle \cos^2\theta \rangle +$$
$$[-3 + 9\langle \cos^2\gamma \rangle]\langle \cos^4\theta \rangle\}\mu^2\nu^2 E_y^2 \quad (8)$$

$$I_{s,p} = \langle \mu_y^2 \nu_x^2 \rangle E_y^2 = \frac{1}{16}\{[3 - \langle \cos^2\gamma \rangle] +$$
$$[-2 - 2\langle \cos^2\gamma \rangle]\langle \cos^2\theta \rangle +$$
$$[-1 + 3\langle \cos^2\gamma \rangle]\langle \cos^4\theta \rangle\}\mu^2\nu^2 E_y^2 \quad (9)$$

$$I_{p,p} = \langle \mu_x^2 \nu_x^2 \rangle E_x^2 + \langle \mu_z^2 \nu_x^2 \rangle E_z^2 = \frac{1}{16}\{[1 + 5\langle \cos^2\gamma \rangle] +$$
$$[2 - 14\langle \cos^2\gamma \rangle]\langle \cos^2\theta \rangle +$$
$$[-3 + 9\langle \cos^2\gamma \rangle]\langle \cos^4\theta \rangle\}\mu^2\nu^2 E_x^2 +$$
$$\frac{4}{16}\{[1 + \langle \cos^2\gamma \rangle]\langle \cos^2\theta \rangle +$$
$$[1 - 3\langle \cos^2\gamma \rangle]\langle \cos^4\theta \rangle\}\mu^2\nu^2 E_z^2 \quad (10)$$

$$I_{p,s} = \langle \mu_x^2 \nu_y^2 \rangle E_x^2 + \langle \mu_z^2 \nu_y^2 \rangle E_z^2 = \frac{1}{16}\{[3 - \langle \cos^2\gamma \rangle] +$$
$$[-2 - 2\langle \cos^2\gamma \rangle]\langle \cos^2\theta \rangle +$$
$$[-1 + 3\langle \cos^2\gamma \rangle]\langle \cos^4\theta \rangle\}\mu^2\nu^2 E_x^2 +$$
$$\frac{4}{16}\{[1 + \langle \cos^2\gamma \rangle]\langle \cos^2\theta \rangle +$$
$$[1 - 3\langle \cos^2\gamma \rangle]\langle \cos^4\theta \rangle\}\mu^2\nu^2 E_z^2 \quad (11)$$

where E_x^2, E_y^2, and E_z^2 are the electric field intensities in the molecular film along the x, y, and z directions. It is worth noting a few points in eqs 8−11:

(a)

$$\langle \mu_y^2 \nu_y^2 \rangle = \langle \mu_x^2 \nu_x^2 \rangle = \frac{1}{16}\{[1 + 5\langle \cos^2\gamma \rangle] +$$
$$[2 - 14\langle \cos^2\gamma \rangle]\langle \cos^2\theta \rangle + [-3 + 9\langle \cos^2\gamma \rangle]\langle \cos^4\theta \rangle\}\mu^2\nu^2 \quad (12)$$

(b)

$$\langle \mu_y^2 \nu_x^2 \rangle = \langle \mu_x^2 \nu_y^2 \rangle = \frac{1}{16}\{[3 - \langle \cos^2\gamma \rangle] +$$
$$[-2 - 2\langle \cos^2\gamma \rangle]\langle \cos^2\theta \rangle + [-1 + 3\langle \cos^2\gamma \rangle]\langle \cos^4\theta \rangle\}\mu^2\nu^2 \quad (13)$$

(c)

$$\langle \mu_z^2 \nu_x^2 \rangle = \langle \mu_z^2 \nu_y^2 \rangle = \frac{4}{16}\{[1 + \langle \cos^2\gamma \rangle]\langle \cos^2\theta \rangle +$$
$$[1 - 3\langle \cos^2\gamma \rangle]\langle \cos^4\theta \rangle\}\mu^2\nu^2 \quad (14)$$

The results a−c above express the complete symmetry between the in-plane x and y components; in the Appendix, we derive expressions analogous to eqs 8−11 for the case of a circular absorber molecule and find identical symmetry.

(d) If the absorption and emission dipoles are collinear, then $\langle \cos^2\gamma \rangle = 1$ and

$$\langle \mu_y^2 \nu_y^2 \rangle = \langle \mu_x^2 \nu_x^2 \rangle = 3\langle \mu_y^2 \nu_x^2 \rangle = 3\langle \mu_x^2 \nu_y^2 \rangle \quad (15)$$

(e) If the emission dipoles are completely depolarized (randomized), for example, due to internal and/or Brownian motions of the fluorophores, then $\langle \cos^2\gamma \rangle = 1/3$ and all four polarized fluorescence intensities, $I_{a,e}$, will be completely independent of $\langle \cos^4\theta \rangle$; in addition, $I_{s,s} = I_{s,p}$ and $I_{p,p} = I_{p,s}$. As

one would expect for complete depolarization, polarized fluorescence measurements do not add any extra orientation information and we can only determine the second order parameter, $\langle P_2(\cos\theta)\rangle$, which is related to the polarized absorption process.

(f) From eqs 8 and 9, we can determine the fluorescence anisotropy, r, for an ordered system by

$$r \equiv \frac{I_{s,s} - I_{s,p}}{I_{s,s} + 2I_{s,p}} = \frac{[1 - 2\langle\cos^2\theta\rangle + \langle\cos^4\theta\rangle][-2 + 6\langle\cos^2\gamma\rangle]}{[7 + 3\langle\cos^2\gamma\rangle] - 2[1 + 9\langle\cos^2\gamma\rangle]\langle\cos^2\theta\rangle + 5[-1 + 3\langle\cos^2\gamma\rangle]\langle\cos^4\theta\rangle} \tag{16}$$

which for an isotropic molecular assembly, where $\langle\cos^2\theta\rangle = {}^1\!/_3$ and $\langle\cos^4\theta\rangle = {}^1\!/_5$, reduces to the usual relation:

$$r = \frac{2}{5}\left[\frac{3}{2}\langle\cos^2\gamma\rangle - \frac{1}{2}\right] = \frac{2}{5}\langle P_2(\cos^2\gamma)\rangle \tag{17}$$

Returning to the general case expressed in eqs 8−11, we observe that eqs 10 and 11 can be simplified by noting that the electric fields along the x and z directions are related to the magnetic field H_y through the following equations:[52]

$$E_x^{\ 2} = (N^2 - n_c^{\ 2})\frac{H_y^{\ 2}}{(\epsilon_c c)^2} \tag{18}$$

$$E_z^{\ 2} = \left(\frac{n_c}{n_f}\right)^4 N^2 \frac{H_y^{\ 2}}{(\epsilon_c c)^2} \tag{19}$$

where n_f is the refractive index of the molecular film, n_c is the refractive index of the medium above the film, and N is the effective index of the propagating beam (also called Snell's invariant), which is determined by the propagation angle of the incident beam and was defined in previous papers.[3,53]

By combining eqs 8 and 9, we obtain

$$\{[3 - \langle\cos^2\gamma\rangle] + [-2 - 2\langle\cos^2\gamma\rangle]\langle\cos^2\theta\rangle + [-1 + 3\langle\cos^2\gamma\rangle]\langle\cos^4\theta\rangle\}I_{s,s} = \{[1 + 5\langle\cos^2\gamma\rangle] + [2 - 14\langle\cos^2\gamma\rangle]\langle\cos^2\theta\rangle +$$
$$[-3 + 9\langle\cos^2\gamma\rangle]\langle\cos^4\theta\rangle\}I_{s,p} \tag{20}$$

Similarly, by combining eqs 10 and 11, and using eqs 18 and 19, we obtain

$$I_{p,p}(N^2 - n_c^{\ 2})\{[3 - \langle\cos^2\gamma\rangle] + [-2 - 2\langle\cos^2\gamma\rangle]\langle\cos^2\theta\rangle + [-1 + 3\langle\cos^2\gamma\rangle]\langle\cos^4\theta\rangle\} +$$
$$I_{p,p}\left(\frac{n_c}{n_f}\right)^4 N^2\{[4 + 4\langle\cos^2\gamma\rangle]\langle\cos^2\theta\rangle + [4 - 12\langle\cos^2\gamma\rangle]\langle\cos^4\theta\rangle\} = I_{p,s}(N^2 - n_c^{\ 2})\{[1 + 5\langle\cos^2\gamma\rangle] + [2 - 14\langle\cos^2\gamma\rangle]\langle\cos^2\theta\rangle +$$
$$[-3 + 9\langle\cos^2\gamma\rangle]\langle\cos^4\theta\rangle\} + I_{p,s}\left(\frac{n_c}{n_f}\right)^4 N^2\{[4 + 4\langle\cos^2\gamma\rangle]\langle\cos^2\theta\rangle + [4 - 12\langle\cos^2\gamma\rangle]\langle\cos^4\theta\rangle\} \tag{21}$$

As can be observed above, eqs 20 and 21 no longer depend on E_x^2, E_y^2, and E_z^2; thus, collecting four different fluorescence intensities eliminates the need to determine the evanescent field intensities in the molecular film. Equations 20 and 21 relate three unknowns: $\langle\cos^2\theta\rangle$, $\langle\cos^4\theta\rangle$, and $\langle\cos^2\gamma\rangle$. Mathematically, two approaches are possible at this point: one option (method A) is to use a value for $\langle\cos^2\gamma\rangle$ (either assumed on the basis of some theoretical hypothesis or experimentally measured by another technique) and solve eqs 20 and 21 for $\langle\cos^2\theta\rangle$ and $\langle\cos^4\theta\rangle$ to get

$$\langle\cos^2\theta\rangle = \frac{2(N^2 - n_c^{\ 2})(I_{pp}I_{sp} - I_{ss}I_{ps})(-1 + \langle\cos^2\gamma\rangle) - \left(\frac{n_c}{n_f}\right)^4 N^2(I_{pp} - I_{ps})[I_{ss}(-3 + \langle\cos^2\gamma\rangle) + I_{sp}(1 + 5\langle\cos^2\gamma\rangle)]}{2(N^2 - n_c^{\ 2})(I_{pp}I_{sp} - I_{ss}I_{ps})(-1 + \langle\cos^2\gamma\rangle) - \left(\frac{n_c}{n_f}\right)^4 N^2(I_{pp} - I_{ps})[I_{ss}(-1 - \langle\cos^2\gamma\rangle) + I_{sp}(-5 + 11\langle\cos^2\gamma\rangle)]} \tag{22}$$

$$\langle\cos^4\theta\rangle =$$
$$\frac{2(N^2 - n_c^{\ 2})(I_{pp}I_{sp} - I_{ss}I_{ps})(1 - 4\langle\cos^2\gamma\rangle + 3\langle\cos^2\gamma\rangle^2) - \left(\frac{n_c}{n_f}\right)^4 N^2(I_{pp} - I_{ps})(1 + \langle\cos^2\gamma\rangle)[I_{ss}(-3 + \langle\cos^2\gamma\rangle) + I_{sp}(1 + 5\langle\cos^2\gamma\rangle)]}{(-1 + 3\langle\cos^2\gamma\rangle)\left[2(N^2 - n_c^{\ 2})(I_{pp}I_{sp} - I_{ss}I_{ps})(-1 + \langle\cos^2\gamma\rangle) - \left(\frac{n_c}{n_f}\right)^4 N^2(I_{pp} - I_{ps})[I_{ss}(-1 - \langle\cos^2\gamma\rangle) + I_{sp}(-5 + 11\langle\cos^2\gamma\rangle)]\right]} \tag{23}$$

Alternatively, a second option (method B) is to use an independently determined value for $\langle\cos^2\theta\rangle$ (most likely measured experimentally by another technique such as ATR[2,3]) and solve eqs 20 and 21 for $\langle\cos^4\theta\rangle$ and $\langle\cos^2\gamma\rangle$ to get

Molecular Orientation in Thin Films

J. Phys. Chem. B, Vol. 110, No. 13, 2006 **6725**

$$\langle \cos^4 \theta \rangle = \frac{(N^2 - n_c^2)(I_{pp}I_{sp} - I_{ps}I_{ss})(1 - 3\langle \cos^2 \theta \rangle + 2\langle \cos^2 \theta \rangle^2) - \left(\frac{n_c}{n_f}\right)^4 N^2(I_{pp} - I_{ps})\langle \cos^2 \theta \rangle(-I_{sp} - I_{ss} + 4I_{sp}\langle \cos^2 \theta \rangle)}{(N^2 - n_c^2)(I_{pp}I_{sp} - I_{ps}I_{ss})(-1 + \langle \cos^2 \theta \rangle) - \left(\frac{n_c}{n_f}\right)^4 N^2(I_{pp} - I_{ps})[I_{ss}(-2 + \langle \cos^2 \theta \rangle) + I_{sp}(2 + \langle \cos^2 \theta \rangle)]} \tag{24}$$

$$\langle \cos^2 \gamma \rangle = \frac{2(N^2 - n_c^2)(I_{pp}I_{sp} - I_{ps}I_{ss})(-1 + \langle \cos^2 \theta \rangle) - \left(\frac{n_c}{n_f}\right)^4 N^2(I_{pp} - I_{ps})[I_{ss}(-3 + \langle \cos^2 \theta \rangle) + I_{sp}(1 + 5\langle \cos^2 \theta \rangle)]}{2(N^2 - n_c^2)(I_{pp}I_{sp} - I_{ps}I_{ss})(-1 + \langle \cos^2 \theta \rangle) - \left(\frac{n_c}{n_f}\right)^4 N^2(I_{pp} - I_{ps})[I_{ss}(-1 - \langle \cos^2 \theta \rangle) + I_{sp}(-5 + 11\langle \cos^2 \theta \rangle)]} \tag{25}$$

The eqs derived above are for the case of a linear absorber; analogous equations for a circular absorber are derived in the Appendix of this paper. In both cases, the second and fourth order parameters, which are defined as the mean value of the second, $\langle P_2(\cos \theta) \rangle$, and fourth, $\langle P_4(\cos \theta) \rangle$, terms of the Legendre polynomials, can then be calculated from the values of $\langle \cos^2 \theta \rangle$ and $\langle \cos^4 \theta \rangle$ by

$$\langle P_2(\cos \theta) \rangle = \frac{3}{2}\langle \cos^2 \theta \rangle - \frac{1}{2} \tag{26}$$

$$\langle P_4(\cos \theta) \rangle = \frac{35}{8}\langle \cos^4 \theta \rangle - \frac{15}{4}\langle \cos^2 \theta \rangle + \frac{3}{8} \tag{27}$$

2.2. Orientation Order Parameters. Thus far, we have described the orientation order parameters of the dipoles with respect to the lab coordinate system through a set of Euler rotation matrices given in eq 5. Such an orientation can be the overall result of several discrete factors.[54,55] As shown in Figure 3, we consider below three possible factors:

(a) $R(\phi_1, \theta_1, \alpha_1)$, which describes the orientation of the absorption and emission dipoles with respect to the molecular coordinate system,

(b) $R(\phi_2, \theta_2, \alpha_2)$, which describes the orientation of the molecular coordinate system with respect to the local coordinate system, and

(c) $R(\phi_3, \theta_3, \alpha_3)$, which describes the orientation of the local coordinate system (which may be different from the lab coordinate system due to roughness features larger than the individual molecules in the film) with respect to the lab coordinate system. This term describes the effects of surface roughness on the experimental results.

The contributions of all effects are translated into the experimental results, $R(\theta, \phi, \alpha)$, through the expression

$$R(\phi, \theta, \alpha) = R(\phi_3, \theta_3, \alpha_3) \cdot R(\phi_2, \theta_2, \alpha_2) \cdot R(\phi_1, \theta_1, \alpha_1) \tag{28}$$

and by assuming axial symmetry in ϕ_1 and ϕ_2, we get

$$\langle P_{2n}(\cos \theta) \rangle = \langle P_{2n}(\cos \theta_3) \rangle \langle P_{2n}(\cos \theta_2) \rangle \langle P_{2n}(\cos \theta_1) \rangle \tag{29}$$

for $2n = 2, 4, 6, ...$ The result above is a consequence of the sum of spherical harmonics.[56] For the specific case of $2n = 2$, the expression reproduces the result already reported by others[54] and later derived by Simpson and Rowlen using a different approach to account for surface roughness effects on the second order parameter, $\langle P_2(\cos \theta) \rangle$.[55] Here, we also extend the expression for any even order parameter, as TIRF experimental results also contain information on $\langle P_4(\cos \theta) \rangle$. The experimentally determined order parameters relating to θ (the angle between the absorption dipole and the lab surface normal) inherently include these factors, so it is useful to be able to factor them out in order to recover the distribution of the molecule with respect to the local surface plane.

2.3. Orientation Distribution Based on the Maximum Entropy Method. All of the information on the order parameters obtained above is determined directly from experimental measurements, and the calculations do not invoke any model for the molecular orientation distribution. In this section, we will employ concepts of statistics to construct an orientation distribution function that will describe the probability of having molecules tilted at every angle. We aim to do that when only a few pieces of information (i.e., a few order parameters) have been experimentally determined. This scenario is a typical problem in statistics (and in information theory) in which a maximum entropy approach is used to provide the most random probability function that is consistent with a given set of information[49] and can be applied to any amount of available information. According to the maximum entropy method,[49] the probability distribution can be described by

$$N(\theta) = e^{[-1 + \mu + \sum_{i=1}^{m} \lambda_i g_i(\theta)]} \tag{30}$$

where $g_i(\theta)$ (for $i = 1, ..., m$) are the experimentally determined (or known) information about the system, λ_i are the associated Lagrange multipliers, m is an integer defining the number of known order parameters, and μ is related to the normalization of the probability function
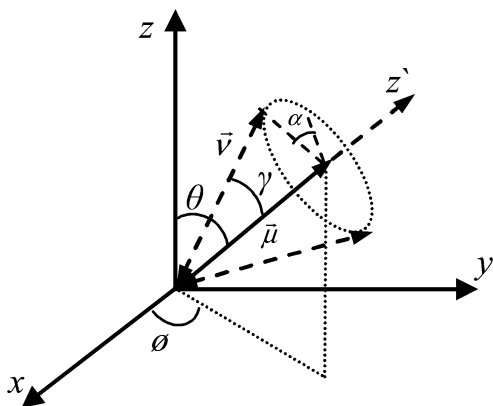
$$\int_0^\pi N(\theta) \sin \theta \, d\theta = 1 \tag{31}$$

6726 *J. Phys. Chem. B, Vol. 110, No. 13, 2006*

Runge et al.

Figure 2. The absorption dipole is defined along the z'-axis for a linear absorber. γ is the angle between the absorption, $\vec{\mu}$, and emission, $\vec{\nu}$, dipoles. The relation between the molecular and laboratory axes is given by the Euler matrices with rotations defined as follows: α is the angle of rotation around the z-axis, θ is a rotation about the y-axis and defines the angle between the lab z-axis and the molecular z'-axis, which is parallel to the absorption dipole, and the angle ϕ is a rotation around the z-axis.
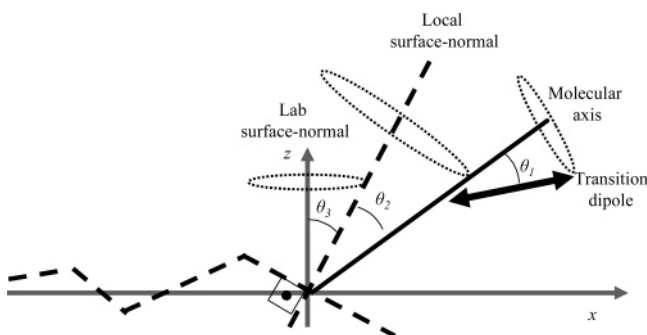

Figure 3. Cross section of the substrate showing the relationship between θ_1, θ_2, and θ_3 projected into the $x-z$ plane.

For the case where only the second order parameter is known, $m = 1$, we have

$$g_1(\theta) = P_2(\cos \theta) \tag{32}$$

and the value of the Lagrange multiplier, λ_2, is found by imposing the experimental information available:

$$\int_0^\pi N(\theta)\, P_2(\cos \theta) \sin \theta \, d\theta =$$

$$\frac{\int_0^\pi e^{\lambda_2 P_2(\cos\theta)} P_2(\cos \theta) \sin \theta \, d\theta}{\int_0^\pi e^{\lambda_2 P_2(\cos \theta)} \sin \theta \, d\theta} = \langle P_2(\cos \theta) \rangle \tag{33}$$

Expression 33 is a transcendental equation that requires a numerical procedure to solve for λ_2; several numerical approaches to treat this sort of problem are readily available in codes such as Mathematica.[57]

For the case where the second and fourth order parameters are known, $m = 2$, we can write

$$g_1(\theta) = P_2(\cos \theta) \tag{34}$$

$$g_2(\theta) = P_4(\cos \theta) \tag{35}$$

with the values of the Lagrange multipliers, λ_2 and λ_4, found by imposing the experimental constraints:

$$\int_0^\pi N(\theta)\, P_2(\cos \theta) \sin \theta \, d\theta =$$

$$\frac{\int_0^\pi e^{\lambda_2 P_2(\cos\theta)+\lambda_4 P_4(\cos\theta)} P_2(\cos \theta) \sin \theta \, d\theta}{\int_0^\pi e^{\lambda_2 P_2(\cos\theta)+\lambda_4 P_4(\cos\theta)} \sin \theta \, d\theta} = \langle P_2(\cos \theta) \rangle \tag{36}$$

$$\int_0^\pi N(\theta)\, P_4(\cos \theta) \sin \theta \, d\theta =$$

$$\frac{\int_0^\pi e^{\lambda_2 P_2(\cos\theta)+\lambda_4 P_4(\cos\theta)} P_4(\cos \theta) \sin \theta \, d\theta}{\int_0^\pi e^{\lambda_2 P_2(\cos\theta)+\lambda_4 P_4(\cos\theta)} \sin \theta \, d\theta} = \langle P_4(\cos \theta) \rangle \tag{37}$$

Again, eqs 36 and 37 require a numerical procedure to determine the values of the Lagrange multipliers. We note here that an alternative approach for eqs 34 and 35 would be to define them in terms of $g_1(\theta) = \cos^2 \theta$ and $g_2(\theta) = \cos^4 \theta$, as they are linearly independent functions, which means that they provide nonredundant information. However, all Legendre terms are orthogonal functions to each other, therefore linearly independent, and provide a straightforward basis to expand as more information becomes available.

For the sake of comparison, we describe a Gaussian distribution by

$$N(\theta) = c e^{[-(\theta - a)^2/2b^2]} \tag{38}$$

for $0 \leq \theta \leq {}^\pi/_2$, with the axial symmetry obtained by assuming $N(\theta) = N(\pi - \theta)$ for ${}^\pi/_2 \leq \theta \leq \pi$. As constant c in eq 38 is determined by normalization of the probability function, the other fitting parameters of the Gaussian distribution, a and b, are found by numerically solving the following eqs imposed by the experimental data:

$$\frac{\int_0^{\pi/2} e^{-((\theta-a)^2/2b^2)} P_2(\cos \theta) \sin \theta \, d\theta}{\int_0^{\pi/2} e^{-((\theta-a)^2/2b^2)} \sin \theta \, d\theta} = \langle P_2(\cos \theta) \rangle \tag{39}$$

$$\frac{\int_0^{\pi/2} e^{-((\theta-a)^2/2b^2)} P_4(\cos \theta) \sin \theta \, d\theta}{\int_0^{\pi/2} e^{-((\theta-a)^2/2b^2)} \sin \theta \, d\theta} = \langle P_4(\cos \theta) \rangle \tag{40}$$

3. Discussion

3.1. Choice of Method for Order Parameter Derivations. Method A (eqs 22 and 23) can be used to determine the second and fourth order parameters from polarized TIRF data. In this case, $\langle \cos^2 \gamma \rangle$ must be assumed, or measured independently.[18,58,59] In most of the literature on this topic, values for $\langle \cos^2 \gamma \rangle$ are determined for the molecule of interest in viscous solutions to eliminate fluorescence depolarization from rotational diffusion of the fluorophores.[27,28,34,60] Equations 24 and 25 show how the fourth order parameter and $\langle \cos^2 \gamma \rangle$ can be calculated from the fluorescence data, provided that the second order parameter is independently measured. Using this method, which we call method B, a value of $\langle \cos^2 \gamma \rangle$ does not need to be assumed or measured independently. Since $\langle \cos^2 \gamma \rangle$ can change significantly depending on the environment of the fluorophore,[31,45,61,62] it is useful to be able to calculate $\langle \cos^2 \gamma \rangle$ directly in the same environment (in this case, an immobilized film at a solid/liquid interface) in which the order parameters are measured.

3.2. Orientation Distribution with One Order Parameter. If only one order parameter is measured experimentally, for

Molecular Orientation in Thin Films

J. Phys. Chem. B, Vol. 110, No. 13, 2006 **6727**

TABLE 1: One Order Parameter Fit with the Maximum Entropy Distribution and the Delta, δ, Distribution[a]

$\langle P_2(\cos\theta)\rangle$	Maximum Entropy Distribution	δ Distribution
-0.5	—	—
-0.35	(figure)	(figure)
-.2	(figure)	(figure)
0	(figure with $0°$, θ, $N(\theta)$, $180°$)	(figure)
0.25	(figure)	(figure)
0.85	(figure)	(figure)
1.0	(figure)	(figure)

[a] Polar plot representations are explained in one of the plots, where the length of the dashed line is proportional to the probability density.

Figure 4. Graph of possible values of $\langle P_2(\cos\theta)\rangle$ and $\langle P_4(\cos\theta)\rangle$. Regions 1 and 2, above the solid line and below the dashed line, respectively, are excluded because these combinations of $\langle P_2(\cos\theta)\rangle$ and $\langle P_4(\cos\theta)\rangle$ values are not possible. The dashed line indicates the combinations that are well-defined by the delta distribution. The three vertical lines (a, b, and c) show the values of $\langle P_2(\cos\theta)\rangle$ and $\langle P_4(\cos\theta)\rangle$ that were used in the calculations shown in Figure 5.

example, $\langle P_2(\cos\theta)\rangle$ from polarized ATR absorbance measurements, the orientation distribution can be determined from eqs 30−33. Table 1 shows the radial plots for the orientation distribution determined for different values of $\langle P_2(\cos\theta)\rangle$ using the maximum entropy method. For comparison, the corresponding orientation distribution determined using a delta function is also shown. As illustrated in Table 1, the delta function describes the most ordered distribution that is consistent with the experimental order parameter, while the maximum entropy method creates the most random distribution of dipoles that also satisfies the same order parameter. When $\langle P_2(\cos\theta)\rangle$ is close to the extremes of -0.5 and 1, the dipoles are either parallel, $\langle\cos^2\theta\rangle = 0$, or perpendicular, $\langle\cos^2\theta\rangle = 1$, to the substrate. At the extreme values of $\langle P_2(\cos\theta)\rangle$, the plots in Table 1 indicate that the distributions created using the two models converge to the same profile and agree well. However, at intermediate values of $-0.5 < \langle P_2(\cos\theta)\rangle < 1$, the two distributions show significantly different profiles, although they both have the same order parameter. Additional order parameters can be logically incorporated into the maximum entropy function to define more details of the distribution profile (as will be shown next).[18,44,61] In comparison, the delta function is completely defined and fixed with just one order parameter, and if the molecular system is not fully ordered, any additional order parameter would show the inconsistency of the delta distribution approach.
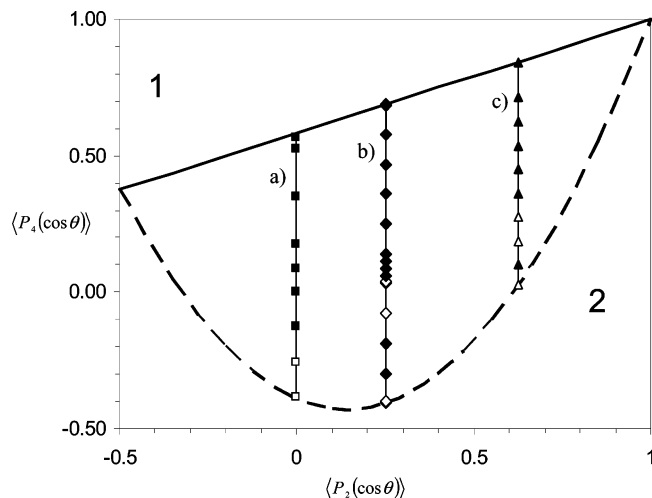
3.3. Orientation Distribution from Two Order Parameters. We now consider a scenario where two order parameters are known; in particular, we deal with the situation where $\langle P_2(\cos\theta)\rangle$ and $\langle P_4(\cos\theta)\rangle$ are determined, although other combinations of order parameters could be treated similarly.[63] Figure 4 shows the mathematical domain of physically meaningful values for $\langle P_2(\cos\theta)\rangle$ and $\langle P_4(\cos\theta)\rangle$. As described in previous works,[11,16,27,64] the two limiting curves of the physical domain are defined by (a, upper curve) $\langle P_4(\cos\theta)\rangle = \frac{5}{12}\langle P_2(\cos\theta)\rangle + \frac{7}{12}$ (which is a consequence of $\langle\cos^4\theta\rangle \leq \langle\cos^2\theta\rangle$) and (b, lower curve) $\langle P_4(\cos\theta)\rangle = \frac{35}{18}\langle P_2(\cos\theta)\rangle^2 - \frac{5}{9}\langle P_2(\cos\theta)\rangle - \frac{7}{18}$ (due to the Schwarz inequality $\langle\cos^4\theta\rangle \geq \langle\cos^2\theta\rangle^2$). This physical domain is established purely on the basis of mathematical arguments and is independent of any orientation distribution; therefore, any valid experimental data, that is, a pair of values given by $\{\langle P_2(\cos\theta)\rangle,\langle P_4(\cos\theta)\rangle\}$, must fall within this area.

Next, we examine the delta, Gaussian, and maximum entropy approaches for describing an orientation distribution for possible values of $\langle P_2(\cos\theta)\rangle$ and $\langle P_4(\cos\theta)\rangle$. As a delta distribution dictates that $\langle\cos^2\theta\rangle^2 = \langle\cos^4\theta\rangle$, this distribution is only consistent with points in the lower limiting curve (dashed line) of Figure 4. Any other point in the two-dimensional physical domain cannot be described by a delta distribution.

The maximum entropy and Gaussian distributions are compared at several points $\{\langle P_2(\cos\theta)\rangle,\langle P_4(\cos\theta)\rangle\}$ of the 2-D domain shown in Figure 4.[11,50,60,64−66] For each point, we have used a Mathematica routine (root-find) to numerically solve for the fitting parameters that are present in the maximum entropy distribution in eqs 36 and 37 (Lagrange coefficients λ_2 and λ_4) and in the Gaussian distribution in eqs 39 and 40 (constants a and b). Once the fitting parameters were determined, the distribution functions were used to recalculate the two order parameters. For the maximum entropy method, the numerical routine could always find a set of λ_2 and λ_4 values that simultaneously solved eqs 36 and 37, while, for the Gaussian approach, the numerical approach had difficulty converging to a solution for a and b to simultaneously satisfy eqs 39 and 40 at several points. To quantify the ability of each distribution to describe a particular point of the 2-D domain, we define an
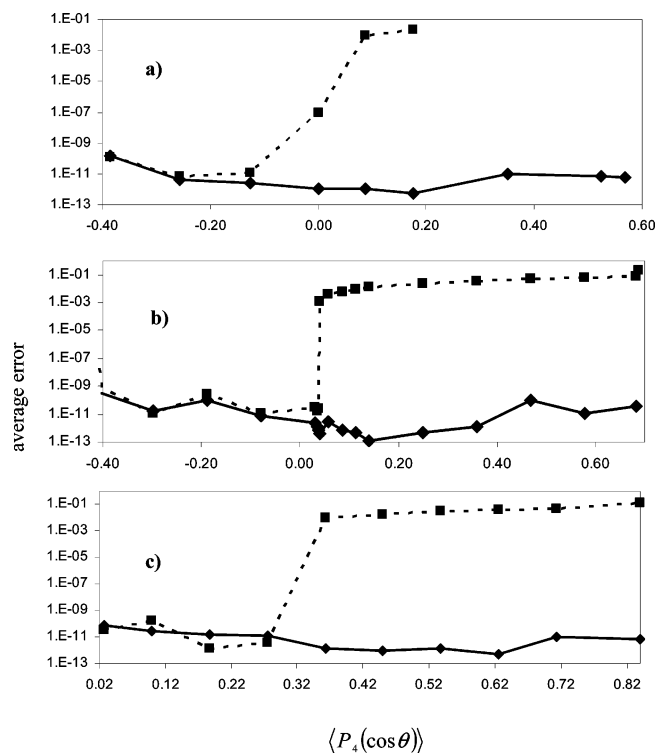
Figure 5. Graphs showing the error for different values of $\langle P_2(\cos \theta)\rangle$: (a) $\langle P_2(\cos \theta)\rangle = 0$, (b) $\langle P_2(\cos \theta)\rangle = 0.25$, and (c) $\langle P_2(\cos \theta)\rangle = 0.625$ for the Gaussian distribution (squares connected by a dashed line) and the maximum entropy method (diamonds connected by a solid line).

TABLE 2: Two Order Parameter Fit with the Maximum Entropy Distribution[a]

-0.35	0	0.25	0.625	0.85
0.4156	0.4375	0.556	0.669	0.806
0.394	0.1313	0.294	0.494	0.719
0.263	0	0.119	0.3625	0.631
0.131	-0.219*	-0.144*	0.1875*	0.5875
0.0875	-0.35*	-0.363*	0.0563*	0.561

[a] Each column is a different $\langle P_2(\cos \theta)\rangle$ value (indicated in the first row), and each box contains an orientation distribution created with the $\langle P_4(\cos \theta)\rangle$ value shown in the box. An asterisk signifies that the fit for the Gaussian distribution is also acceptable.

error function as the sum of the absolute difference between the left-hand side (LHS) and the right-hand side (RHS) of eqs 36 and 37, $|\text{LHS} - \text{RHS}|_{\text{eq36}} + |\text{LHS} - \text{RHS}|_{\text{eq37}}$, for the maximum entropy approach; we apply an identical definition but use the corresponding eqs 39 and 40 for the Gaussian distribution. Figure 5 shows the error for the Gaussian and maximum entropy fittings for three fixed values of $\langle P_2(\cos \theta)\rangle = 0$, 0.25, and 0.625, in plots a, b, and c, respectively, with values of $\langle P_4(\cos \theta)\rangle$ spanning across the whole possible range. From these plots, we observe that the error is always numerically very small for the maximum entropy approach (essentially round-off error); however, for the Gaussian distribution, we can clearly locate a transition between a region that is well fit and a region that cannot be properly fit. For any value of $\langle P_2(\cos \theta)\rangle$, when $\langle P_4(\cos \theta)\rangle$ is close to the lower limiting curve, the fitting is acceptable; however, as $\langle P_4(\cos \theta)\rangle$ approaches roughly the midway point of the allowable range for a fixed $\langle P_2(\cos \theta)\rangle$, then the error sharply increases and the Gaussian distribution is clearly a poor fit beyond that point. Therefore, the region of the physical domain shown in Figure 4 that can be described well with a Gaussian distribution is located near the lower boundary of the whole domain.

Table 2 illustrates the orientation distributions calculated with the maximum entropy method for different combinations of $\langle P_2(\cos \theta)\rangle$ and $\langle P_4(\cos \theta)\rangle$ that span the whole physical domain. For those points in Figure 4 where the Gaussian distribution also provides a good fit (a subregion of the whole physical domain), Table 3 compares the shapes of the distributions determined from the Gaussian and maximum entropy methods. By comparing the orientation distributions in Table 3, we observe that when the Gaussian distribution is successful in achieving a good fit, the shape of its orientation distribution is similar to the one produced by the maximum entropy method.

TABLE 3: Two Order Parameter Fit with the Maximum Entropy Distribution and the Gaussian Distribution

$\langle P_2(\cos \theta)\rangle$	$\langle P_4(\cos \theta)\rangle$	Maximum Entropy Distribution	Gaussian Distribution
0	-0.38		
0	-0.26		
0.25	-0.4		
0.25	-0.078		
0.25	0.037		
0.625	0.03		
0.625	0.19		
0.625	0.28		

Molecular Orientation in Thin Films

J. Phys. Chem. B, Vol. 110, No. 13, 2006 **6729**

While the Gaussian distribution can describe more combinations of order parameters than a delta function, which is strictly confined to lower limiting curve, it still only covers a small region of the full domain of the order parameters. In contrast, the maximum entropy distribution can provide an orientation distribution for every possible combination of order parameters. Near the upper boundary of Figure 4, the a priori shape of the Gaussian distribution cannot describe distributions that have maxima at polar angles of 0 or 90°. The same is true for values of $\langle P_2(\cos\theta)\rangle$ and $\langle P_4(\cos\theta)\rangle$ close to the isotropic values of zero, where the orientation distribution does not have a well-defined maximum, and the Gaussian also fails to provide a reasonable fit.

4. Conclusions

We have described two methods for determining order parameters for a molecular film using polarized fluorescence techniques based on total internal reflection. In method A, fluorescence data are used to determine $\langle P_2(\cos\theta)\rangle$ and $\langle P_4(\cos\theta)\rangle$ by assuming (or independently measuring) a value for $\langle \cos^2\gamma\rangle$. Method B uses the fluorescence data along with an independently measured value of $\langle P_2(\cos\theta)\rangle$ to determine $\langle P_4(\cos\theta)\rangle$ and $\langle \cos^2\gamma\rangle$. The advantage in using the latter approach is that $\langle \cos^2\gamma\rangle$ can be recovered with the chromophores located in the physical/chemical environment of interest (e.g., confined to a solid/liquid interface). Mathematical formalisms for determining the effects of substrate roughness on the even numbered order parameters are also presented. From a pair of experimentally determined order parameters, an orientation distribution can be constructed using the maximum entropy method. We compared the maximum entropy method with two other orientation distribution models, the delta and Gaussian distributions, showing that the maximum entropy method is capable of fitting the physical domain composed of all possible values of $\langle P_2(\cos\theta)\rangle$ and $\langle P_4(\cos\theta)\rangle$, unlike the other two distributions that have significant limitations in their applicability. In the following paper, we apply the formalisms developed here to study cytochrome *c* protein films formed by different techniques (direct adsorption out of solution and microcontact printing) on both dielectric and electroactive substrates (glass and ITO).

Appendix: Fluorescence Intensity Expressions for the Case of a Circular Absorber

In this appendix, we determine analogous equations for a circular absorber,[27,36] with the equations numbered to correspond with those already presented in this paper for the case of a linear absorber. The case of a circular absorber has been reported by Tronin et al.;[33] however, there are errors[67,68] in their auxiliary eqs 12 and 13 that preclude their use for the derivation of the order parameters. In the molecular coordinate system ($x'-$ $y'-z'$), the absorption dipole for a circular absorber can be described as follows:

$$\begin{pmatrix}\mu_{x'}\\\mu_{y'}\\\mu_{z'}\end{pmatrix}=\begin{pmatrix}\mu/\sqrt{2}\\\mu/\sqrt{2}\\0\end{pmatrix} \quad \text{(A2)}$$

and the emission dipole:

$$\begin{pmatrix}\nu_{x'}\\\nu_{y'}\\\nu_{z'}\end{pmatrix}=R(\beta,\gamma)\begin{pmatrix}\nu/\sqrt{2}\\\nu/\sqrt{2}\\0\end{pmatrix} \quad \text{(A3)}$$

with

$$R(\beta,\gamma)\equiv\begin{pmatrix}\cos\beta & 0 & \sin\beta\\0 & 1 & 0\\-\sin\beta & 0 & \cos\beta\end{pmatrix}\begin{pmatrix}\cos\gamma & -\sin\gamma & 0\\\sin\gamma & \cos\gamma & 0\\0 & 0 & 1\end{pmatrix} \quad \text{(A4)}$$

where γ and β account for the in-plane and out-of-plane depolarization, respectively. Neglecting the out-of-plane depolarization, we get

$$I_{s,s}=\langle\mu_y^2\nu_y^2\rangle E_y^2=\frac{1}{64}\{[1+2\langle\cos^2\gamma\rangle]\cdot[3+2\langle\cos^2\theta\rangle+ \\ 3\langle\cos^4\theta\rangle]\}\mu^2\nu^2E_y^2 \quad \text{(A8)}$$

$$I_{s,p}=\langle\mu_y^2\nu_x^2\rangle E_y^2=\frac{1}{64}\{[1+2\langle\cos^2\gamma\rangle]+2[11- \\ 10\langle\cos^2\gamma\rangle]\langle\cos^2\theta\rangle+[1+2\langle\cos^2\gamma\rangle]\langle\cos^4\theta\rangle\}\mu^2\nu^2E_y^2 \quad \text{(A9)}$$

$$I_{p,p}=\langle\mu_x^2\nu_x^2\rangle E_x^2+\langle\mu_z^2\nu_x^2\rangle E_z^2=\frac{1}{64}\{[1+2\langle\cos^2\gamma\rangle][3+ \\ 2\langle\cos^2\theta\rangle+3\langle\cos^4\theta\rangle]\}\mu^2\nu^2E_x^2+\frac{4}{64}\{[3-2\langle\cos^2\gamma\rangle]+ \\ 2[2\langle\cos^2\gamma\rangle-1]\langle\cos^2\theta\rangle-[2\langle\cos^2\gamma\rangle+1]\langle\cos^4\theta\rangle\}\mu^2\nu^2E_z^2 \quad \text{(A10)}$$

$$I_{p,s}=\langle\mu_x^2\nu_y^2\rangle E_x^2+\langle\mu_z^2\nu_y^2\rangle E_z^2=\frac{1}{64}\{[1+2\langle\cos^2\gamma\rangle]+ \\ 2[11-10\langle\cos^2\gamma\rangle]\langle\cos^2\theta\rangle+ \\ [1+2\langle\cos^2\gamma\rangle]\langle\cos^4\theta\rangle\}\mu^2\nu^2E_x^2+ \\ \frac{4}{64}\{[3-2\langle\cos^2\gamma\rangle]+2[2\langle\cos^2\gamma\rangle-1]\langle\cos^2\theta\rangle- \\ [2\langle\cos^2\gamma\rangle+1]\langle\cos^4\theta\rangle\}\mu^2\nu^2E_z^2 \quad \text{(A11)}$$

The expressions above agree with those from Tronin et al.[33,34] after a couple of errors are fixed in their publication. In eqs 12 and 13 of the referenced article,[33,34] the numerical terms $1/4$ and $3/4$ should be associated only with the u term and it should be $((1/4)u+q)$ instead of $(1/4)(u+q)$ and $((3/4)u-q)$ instead of $(3/4)(u-q)$.

6730 *J. Phys. Chem. B, Vol. 110, No. 13, 2006*

Runge et al.

Method A:

$$\langle \cos^2 \theta \rangle = \frac{\left(\frac{n_c}{n_f}\right)^4 N^2 (I_{pp} - I_{ps})(3I_{sp} - I_{ss})}{4(N^2 - n_c{}^2)(I_{pp}I_{sp} - I_{ss}I_{ps})(-1 + \langle \cos^2 \gamma \rangle) - \left(\frac{n_c}{n_f}\right)^4 N^2 (I_{pp} - I_{ps})[I_{ss}(-5 + 4\langle \cos^2 \gamma \rangle) + I_{sp}(-1 + 4\langle \cos^2 \gamma \rangle)]} \tag{A22}$$

$$\langle \cos^4 \theta \rangle =$$

$$\frac{-4(N^2 - n_c{}^2)(I_{pp}I_{sp} - I_{ss}I_{ps})(-1 - \langle \cos^2 \gamma \rangle + 2\langle \cos^2 \gamma \rangle^2) + \left(\frac{n_c}{n_f}\right)^4 N^2 (I_{pp} - I_{ps})[I_{ss}(17 - 26\langle \cos^2 \gamma \rangle + 8\langle \cos^2 \gamma \rangle^2) + I_{sp}(-3 - 2\langle \cos^2 \gamma \rangle + 8\langle \cos^2 \gamma \rangle^2)]}{(1 + 2\langle \cos^2 \gamma \rangle)\left\{ 4(N^2 - n_c{}^2)(I_{pp}I_{sp} - I_{ss}I_{ps})(-1 + \langle \cos^2 \gamma \rangle) - \left(\frac{n_c}{n_f}\right)^4 N^2 (I_{pp} - I_{ps})[I_{ss}(-5 + 4\langle \cos^2 \gamma \rangle) + I_{sp}(-1 + 4\langle \cos^2 \gamma \rangle)]\right\}} \tag{A23}$$

Method B:

$$\langle \cos^4 \theta \rangle =$$

$$\frac{-2(N^2 - n_c{}^2)(I_{pp}I_{sp} - I_{ps}I_{ss})[3\langle \cos^2 \theta \rangle + 2\langle \cos^2 \theta \rangle^2] + N^2 \left(\frac{n_c}{n_f}\right)^4 (I_{pp} - I_{ps})[I_{ss}(1 - 3\langle \cos^2 \theta \rangle - 6\langle \cos^2 \theta \rangle^2) + I_{sp}(-3 + \langle \cos^2 \theta \rangle + 2\langle \cos^2 \theta \rangle^2)]}{6(N^2 - n_c{}^2)(I_{pp}I_{sp} - I_{ps}I_{ss})\langle \cos^2 \theta \rangle - N^2 \left(\frac{n_c}{n_f}\right)^4 (I_{pp} - I_{ps})[I_{ss}(1 + 7\langle \cos^2 \theta \rangle) + 3I_{sp}(-1 + \langle \cos^2 \theta \rangle)]} \tag{A24}$$

$$\langle \cos^2 \gamma \rangle = \frac{4(N^2 - n_c{}^2)(-I_{pp}I_{sp} + I_{ps}I_{ss})\langle \cos^2 \theta \rangle + N^2 \left(\frac{n_c}{n_f}\right)^4 (I_{pp} - I_{ps})[I_{ss} + I_{sp}(-3 + \langle \cos^2 \theta \rangle) + 5I_{ss}\langle \cos^2 \theta \rangle]}{4\langle \cos^2 \theta \rangle \left[N^2 \left(\frac{n_c}{n_f}\right)^4 (I_{pp} - I_{ps})(I_{sp} + I_{ss}) + (N^2 - n_c{}^2)(-I_{pp}I_{sp} + I_{ps}I_{ss})\right]} \tag{A25}$$

References and Notes

(1) Breton, J.; Vermeglio, A. Orientation of Photosynthetic Pigments *in Vivo*. In *Photosynthesis*; Govindjee, Ed.; Academic Press: New York, 1982; Vol. 1, pp 153.

(2) Lafrance, C.; Chabot, P.; Pigeon, M.; Prudhomme, R. E.; Pezolet, M. *Polymer* **1993**, *34*, 5029.

(3) Runge, A. F.; Rasmussen, N. C.; Saavedra, S. S.; Mendes, S. B. *J. Phys. Chem. B* **2005**, *109*, 424.

(4) Bauman, D.; Schulze, H.; Kuball, H. G. *Liq. Cryst.* **2000**, *27*, 1357.

(5) Johansson, L. B. A. *Chem. Phys.* **1985**, *118*, 516.

(6) Johansson, L. B. A.; Lindblom, G. *Q. Rev. Biophys.* **1980**, *13*, 63.

(7) van Gurp, M.; van Ginkel, G.; Levine, Y. K. *J. Theor. Biol.* **1988**, *131*, 333.

(8) Ge, J. J.; Li, C. Y.; Xue, G.; Mann, I. K.; Zhang, D.; Wang, S.-Y.; Harris, F. W.; Cheng, S. Z. D.; Hong, S.-C.; Zhuang, X.; Shen, Y. R. *J. Am. Chem. Soc.* **2001**, *123*, 5768.

(9) Oh-e, M.; Hong, S.-C.; Shen, Y. R. *J. Phys. Chem. B* **2000**, *104*, 7455.

(10) Labarthet, F. L.; Buffeteau, T.; Sourisseau, C. *J. Phys. Chem. B* **1998**, *102*, 5754.

(11) Labarthet, F. L.; Buffeteau, T.; Sourisseau, C. *Appl. Spectrosc.* **2000**, *54*, 699.

(12) Labarthet, F. L.; Bruneel, J. L.; Buffeteau, T.; Sourisseau, C. *J. Phys. Chem. B* **2004**, *108*, 6949.

(13) Rousseau, M.; Lefevre, T.; Beaulieu, L.; Asakura, T.; Pezolet, M. *Biomacromolecules* **2004**, *5*, 2247.

(14) Chapoy, L. L.; DuPrè, D. B. *J. Chem. Phys.* **1978**, *69*, 519.

(15) Chapoy, L. L.; DuPrè, D. B. *J. Chem. Phys.* **1979**, *70*, 2550.

(16) Kooyman, R. P. H.; Levine, Y. K.; Van der Meer, B. W. *Chem. Phys.* **1981**, *60*, 317.

(17) van der Meer, B. W.; Kooyman, R. P. H.; Levine, Y. K. *Chem. Phys.* **1982**, *66*, 39.

(18) Mulders, F.; van Langen, H.; van Ginkel, G.; Levine, Y. K. *Biochim. Biophys. Acta* **1986**, *859*, 209.

(19) van Langen, H.; Engelen, D.; van Ginkel, G.; Levine, Y. K. *Chem. Phys. Lett.* **1987**, *138*, 99.

(20) van Langen, H.; Schrama, C. A.; van Ginkel, G.; Ranke, G.; Levine, Y. K. *Biophys. J.* **1989**, *55*, 937.

(21) van Langen, H.; van Ginkel, G.; Levine, Y. K. *Chem. Phys.* **1989**, *130*, 271.

(22) van Gurp, M.; Levine, Y. K. *Chem. Phys. Lett.* **1991**, *180*, 349.

(23) van Zandvoort, M. A. M. J.; Gerritsen, H. C.; van Ginkel, G.; Levine, Y. K.; Tarroni, R.; Zannoni, C. *J. Phys. Chem. B* **1997**, *101*, 4149.

(24) LeGrange, J. D.; Riegler, H. E.; Zurawsky, W. P.; Scarlata, S. F. *Thin Solid Films* **1988**, *159*, 101.

(25) LeGrange, J. D.; Riegler, H. E.; Zurawsky, W. P.; Scarlata, S. F. *J. Chem. Phys.* **1989**, *90*, 3838.

(26) Fraaije, J. G. E. M.; Kleijn, J. M.; van der Graaf, M.; Dijt, J. C. *Biophys. J.* **1990**, *57*, 965.

(27) Bos, M. A.; Kleijn, J. M. *Biophys. J.* **1995**, *68*, 2566.

(28) Bos, M. A.; Kleijn, J. M. *Biophys. J.* **1995**, *68*, 2573.

(29) Bos, M. A.; Werkhoven, T. M.; Kleijn, J. M. *Langmuir* **1996**, *12*, 3980.

(30) Zhai, X.; Kleijn, J. M. *Biophys. J.* **1997**, *72*, 2651.

(31) Yang, J.; Kleijn, J. M. *Biophys. J.* **1999**, *76*, 323.

(32) Thompson, N. L.; Burghardt, T. P. *Biophys. Chem.* **1986**, *25*, 91.

(33) Tronin, A.; Strzalka, J.; Chen, X.; Dutton, P. L.; Blasie, J. K. *Langmuir* **2000**, *16*, 9878.

(34) Tronin, A.; Edwards, A. M.; Wright, W. W.; Vanderkooi, J. M.; Blasie, J. K. *Biophys. J.* **2002**, *82*, 996.

(35) Edmiston, P. L.; Lee, J. E.; Wood, L. L.; Saavedra, S. S. *J. Phys. Chem.* **1996**, *100*, 775.

(36) Edmiston, P. L.; Lee, J. E.; Cheng, S.; Saavedra, S. S. *J. Am. Chem. Soc.* **1997**, *119*, 560.

(37) Cheng, Y.-Y.; Lin, S. H.; Chang, H.-C.; Su, M.-C. *J. Phys. Chem. A* **2003**, *107*, 10687.

(38) Fujita, K.; Nakamura, F.; Ohno, H. *Polym. Adv. Technol.* **2004**, *15*, 567.

(39) Jang, W.; Miller, J. D. *J. Phys. Chem.* **1995**, *99*, 10272.

(40) Lee, J. E.; Saavedra, S. S. Molecular Orientation in Absorbed Cytochrome *c* Films by Planar Waveguide Linear Dichroism. In *Proteins at Interfaces II: Fundamentals and Applications*; Horbett, T. A., Brash, J. L., Eds.; American Chemical Society: Washington, DC, 1995; p 269.

(41) Lee, J. E.; Saavedra, S. S. *Langmuir* **1996**, *12*, 4025.

(42) Cropek, D. M.; Bohn, P. W. *J. Phys. Chem.* **1990**, *94*, 6452.

(43) Wang, J.; Paszti, Z.; Even, M. A.; Chen, Z. *J. Phys. Chem. B* **2004**, *108*, 3625.

(44) Bower, D. I. *J. Polym. Sci., Polym. Phys. Ed.* **1981**, *19*, 93.

(45) van Ginkel, G.; Korstanje, L. J.; van Langen, H.; Levine, Y. K. *Faraday Discuss. Chem. Soc.* **1986**, *81*, 49.

(46) Axelsen, P. H.; Citra, M. J. *Prog. Biophys. Mol. Biol.* **1996**, *66*, 227.

(47) Adler, M.; Tritton, T. R. *Biophys. J.* **1988**, *53*, 989.

(48) Berne, B. J. Time-Dependent Properties of Condensed Media. In *Physical Chemistry An Advanced Treaty*; Eyring, H., Henderson, D., Jost, W., Eds.; Academic Press: New York, 1971; Vol. 8B.

(49) Frieden, B. R. *Probability, Statistical Optics, and Data Testing*; Springer-Verlag: New York, 1991.

(50) Pottel, H.; Herreman, W.; van der Meer, B. W.; Ameloot, M. *Chem. Phys.* **1986**, *102*, 37.

Molecular Orientation in Thin Films

J. Phys. Chem. B, Vol. 110, No. 13, 2006 **6731**

(51) Zannoni, C.; Arcioni, A.; Cavatorta, P. *Chem. Phys. Lipids* **1983**, *32*, 179.

(52) Mendes, S. B.; Bradshaw, J. T.; Saavedra, S. S. *Appl. Opt.* **2004**, *43*, 70.

(53) Mendes, S. B.; Li, L. F.; Burke, J. J.; Lee, J. E.; Saavedra, S. S. *Appl. Opt.* **1995**, *34*, 6180.

(54) Rothschild, K. J.; Clark, N. A. *Biophys. J.* **1979**, *25*, 473.

(55) Simpson, G. J.; Rowlen, K. L. *J. Phys. Chem. B* **1999**, *103*, 3800.

(56) Arfken, G. *Mathematical Methods for Physicists*, 3rd ed.; Academic Press: San Diego, CA, 1985.

(57) Wolfram, S. *The Mathematica book*, 4th ed.; Wolfram Media: Champaign, IL, 1999.

(58) Lettinga, M. P.; Zuilhof, H.; van Zandvoort, M. A. M. J. *Chem. Phys. Phys. Chem.* **2000**, *2*, 3697.

(59) Kawski, A. *Crit. Rev. Anal. Chem.* **1993**, *23*, 459.

(60) Ameloot, M.; Hendrickx, H.; Herreman, W.; Pottel, H.; van Cauwelaert, F. V. *Biophys. J.* **1984**, *46*, 525.

(61) Vos, M. H.; Kooyman, R. P. H.; Levine, Y. K. *Biochem. Biophys. Res. Commun.* **1983**, *116*, 462.

(62) Kooyman, R. P. H.; Vos, M. H.; Levine, Y. K. *Chem. Phys.* **1983**, *81*, 461.

(63) Wang, J.; Paszti, Z.; Even, M. A.; Chen, Z. *J. Am. Chem. Soc.* **2002**, *124*, 7016.

(64) van de Ven, M. J. M.; Levine, Y. K. *Biochim. Biophys. Acta* **1984**, *777*, 283.

(65) van der Meer, W.; Pottel, H.; Herreman, W.; Ameloot, M.; Hendrickx, H.; Schroder, H. *Biophys. J.* **1984**, *46*, 515.

(66) Sourisseau, C. *Chem. Rev.* **2004**, *104*, 3851.

(67) Tronin, A. Personal communication.

(68) Tronin, A.; Xu, T.; Blasie, J. K. *Langmuir* **2005**, *21*, 7760.